Published in final edited form as:
Sci Signal. ; 6(301): ra98. doi:10.1126/scisignal.2004427.

Regulation of Epithelial Morphogenesis by the G-Protein Coupled Receptor Mist and its Ligand Fog*

Alyssa J. Manning[1,4], **Kimberly A. Peters**[1,4], **Mark Peifer**[1,2], and **Stephen L. Rogers**[1,2,3]

[1]Department of Biology, The University of North Carolina at Chapel Hill, CB# 3280, Fordham Hall, South Road, Chapel Hill, NC 27599-3280, USA

[2]Lineberger Comprehensive Cancer Center

[3]Carolina Center for Genome Sciences

Abstract

Epithelial morphogenesis is essential for shaping organs and tissues and for establishment of the three embryonic germ layers during gastrulation. Studies of gastrulation in *Drosophila* have provided insight into how epithelial morphogenesis is governed by developmental patterning mechanisms. We developed an assay to recapitulate morphogenetic shape changes in individual cultured cells, and used RNAi-based screening to identify Mist, a *Drosophila* G protein-coupled receptor (GPCR) that transduces signals from the secreted ligand Folded gastrulation (Fog) in cultured cells. Mist functioned in Fog-dependent embryonic morphogenesis, and the transcription factor Snail regulated expression of *mist* in zygotes. Our data revealed how a cell fate transcriptional program acts through a ligand-GPCR pair to stimulate epithelial morphogenetic shape changes.

Introduction

During embryogenesis, the developmental program sculpts sheets of epithelial cells to build organs, define tissue compartments, and establish the embryonic body plan. Forces driving these tissue-level rearrangements are produced by the actin and myosin cytoskeleton acting within individual cells and are transmitted from cell to cell within epithelia by adherens junctions (1,2). Cell and tissue shape changes are regulated by a complex interplay between maternally supplied proteins and patterned zygotic gene expression. Understanding how developmental patterning organizes cytoskeletal processes with spatial precision is a key question in the field of developmental biology (3).

G-protein coupled receptors (GPCRs) are one of the largest groups of proteins found in the human genome, yet there are few examples of GPCRs regulating morphogenesis. Genetic analyses in *Drosophila* have revealed a possible example involving a pathway that triggers

Correspondence should be addressed to: S.L.R. (srogers@bio.unc.edu).
[4]These authors contributed equally to this work.

Author contributions: A.J.M, K.A.P. and M.P. performed the experiments and analyzed the data; and A.J.M., K.A.P., M.P., and S.L.R. conceived the project, designed the experiments, and wrote the manuscript.

Competing interests: The authors declare that they have no competing interests.

epithelial folding through apical constriction during gastrulation and salivary gland invagination downstream of the secreted protein Folded gastrulation (Fog) (4, 5). This pathway is thought to involve a GPCR, because the $G\alpha_{12/13}$ homologue Concertina (Cta) is an integral component of the pathway. However, because GPCR-independent activities of G-proteins can also regulate the cytoskeleton (6–8), it is unclear whether GPCRs are involved in initiating apical constriction.

Downstream of Fog, Cta activates RhoGEF2, which is recruited to the apical membrane by the transmembrane protein T48 (9, 10). RhoGEF2 then activates the small GTPase Rho1 to recruit and stimulate cytoskeletal contractile machinery, including Rho kinase (Rok), non-muscle myosin II, and actin, thereby inducing apical constriction (10–13). This pathway is best characterized during gastrulation where it initiates formation of both the ventral furrow, to internalize mesoderm, and the posterior midgut, to internalize endoderm (14). It has been a paradigm for morphogenesis from the level of gene expression to cytoskeletal regulation. Fog is thought to act as a ligand to initiate this signaling pathway, but a receptor for Fog has remained elusive despite many years of genetic and cell biological analysis (5, 11).

Results

Mist transduces Fog signal in cell culture

We developed a novel functional genomic approach to identify Fog receptors by reconstituting the pathway in a cell-based assay. We previously found that activating the downstream effector Rho1 in cultured *Drosophila* S2 cells induces a characteristic contracted morphology (9). We engineered S2 cells to express Fog, and used conditioned medium from these cells to screen several immortalized *Drosophila* cell lines for a contractile response. S2R+ cells exhibited robust contraction in response to Fog, including actin rearrangement and increased phosphorylation of myosin regulatory light chain (Spaghetti squash; Sqh), whereas S2 cells and several other epithelial-derived cell lines failed to respond (Fig. 1A and movie S1). RNAi-mediated depletion of proteins that act in the epithelial folding pathway, including Cta, RhoGEF2, or Rho1, prevented Fog-induced S2R+ cell contraction, suggesting that we had recapitulated this morphogenetic cascade in cultured cells (Fig. 1B).

To identify a receptor that acts downstream of Fog, we performed a targeted RNAi screen, individually depleting the 138 known and predicted GPCRs in the *Drosophila* genome (table S1) (15, 16), and looked for cell contraction in response to Fog. Among the candidates, only two independent dsRNAs corresponding to the uncharacterized gene CG4521 (*methuselah-like 1*) consistently blocked Fog-induced contraction (Fig. 1C). This gene, which we called *mesoderm-invagination signal transducer* (*mist*), encodes a predicted GPCR of the secretin family. Mist is predicted to have a large N-terminal extracellular domain characteristic of this family, seven membrane-spanning helices, and a cytoplasmic C-terminal domain (Fig. 1D). We generated antibodies to Mist that recognized a single protein band on immunoblots of S2R+ cells, a band that was not present in S2R+ cells treated with *mist* dsRNA (fig. S1A). Consistent with the hypothesis that Mist is a Fog receptor, S2R+ cells overexpressing Mist-GFP showed increased amounts of Fog on the plasma membrane when treated at 4°C to block endocytosis compared to S2R+ cells expressing GFP alone (Fig. 1, E and F).

We next addressed whether Mist was sufficient to confer Fog responsiveness to nonresponsive cells. Mist was not detectable in S2 cells and these cells did not respond to Fog (Fig. 1C and fig. S1B). However, ectopic expression of full-length Mist enabled these cells to contract upon treatment with Fog (Fig. 1, C and G). To define the domains required for Fog responsiveness we created Mist deletion constructs that retain the signal sequence but lack the predicted N-terminal extracellular domain (MistΔN), or lack the cytoplasmic domain (MistΔC) (Fig. 1D). MistΔN failed to confer Fog responsiveness upon S2 cells, indicating that the extracellular domain of Mist is required for Fog signaling (Fig. 1C). In contrast, MistΔC conferred Fog responsiveness on S2 cells, indicating the C-terminus is not essential for activating downstream effectors (Fig. 1C). This result is not surprising, because some Gα subunits are activated primarily by intracellular loops of GPCRs (17). Together these data demonstrate that Mist is required for Fog signaling in cultured *Drosophila* cells and that the large extracellular domain of Mist is necessary, perhaps acting as a ligand-binding surface.

Mist is essential for proper *Drosophila* gastrulation

Although these data suggested that Mist can act as a Fog receptor, they did not reveal whether Mist mediates the effects of Fog *in vivo*. Fog was originally identified as a secreted protein that triggers early embryonic movements of gastrulation (5). Thus, we tested the hypothesis that Mist acts as a Fog receptor to induce mesoderm invagination. We first examined whether *mist* is expressed at the right time and place to act in the Fog pathway. *mist* mRNA is present in the blastoderm, suggesting a maternal contribution (Fig. 2A). Just prior to mesoderm invagination, *mist* mRNA abundance was increased specifically along the ventral side and posterior end of the embryo, corresponding to the ventral furrow and posterior midgut primordia (Fig. 2, B–D). Lower amounts of mRNA equivalent to the maternal contribution remained in cells outside this region. *fog* RNA has a different expression pattern and notably, is not expressed in the region between the ventral furrow and posterior midgut (5). *mist* mRNA expression remained strong in the mesoderm and endoderm after invagination (fig. S2A). During ventral furrow invagination, Mist protein was enriched in the same region of the embryo as *mist* mRNA, and localized to the apical surfaces of ventral furrow cells (Fig. 2, E–H; See fig. S3 for antibody control). The increase in *mist* mRNA abundance in the contractile cells of the ventral furrow and posterior midgut primordia just prior to gastrulation is consistent with a role for Mist in the regulation of morphogenesis.

To investigate how the *mist* expression pattern is formed we looked to the embryonic dorso-ventral axis specification pathway, which is initiated by the maternally supplied Dorsal transcription factor. Dorsal acts through the zygotic transcription factors Twist and Snail, both of which are independently required for ventral furrow invagination (18, 19). *fog* is a transcriptional target of Twist in early embryos, but Snail targets involved in ventral furrow invagination remain unclear (5, 20–22). We thus tested the hypothesis that *mist* might be a Twist or Snail target gene. Wild-type embryos exhibited robust expression of *mist* mRNA in the ventral furrow and posterior midgut from the point at which embryos form cells (cellularization) through a process in gastrulation called germ band extension (Fig. 2, I and J insets). When we crossed *snail* heterozygous parents, 25% of embryos, likely *snail*

homozygous mutants, lacked *mist* expression in the ventral furrow but retained expression in the posterior midgut (Fig. 2, I and J). In contrast, most embryos from *twist* heterozygous parents exhibited wild-type *mist* expression, with only a few lacking ventral furrow expression, presumably because Twist enhances *snail* expression in the mesoderm (fig. S2, B and C) (23). These data are consistent with *mist* being regulated by Snail. Given that Snail functions as a transcriptional repressor, its regulation of *mist* expression may be through an indirect transcriptional mechanism.

To test whether Mist functions *in vivo* during gastrulation, we created a mutant with decreased *mist* expression. Imprecise excision of a P-element inserted in the *mist* 5′UTR (fig. S4A) generated a small deletion, which we called $mist^{YO17}$ (fig. S4B), encompassing the promoter, upstream regulatory region, and part of the 5′UTR of *mist*, as well as the coding regions of adjacent genes: the small ribonucleoprotein particle protein *SmG*, the ribosomal subunit *RpS19a*, the unannotated gene CG9777, and the maternally supplied Fog pathway component *rok* (Text S1). The $mist^{YO17}$ mutation is zygotically embryonic lethal and embryos hemizygous for this mutation exhibited substantially reduced *mist* mRNA abundance throughout gastrulation (Fig. 3A and fig. S4C). Further, similar to other Fog pathway mutants (11, 24), $mist^{YO17}$ mutant embryos have reduced apical recruitment of non-muscle myosin heavy chain (Zipper; Zip) within ventral furrow cells and uncoordinated ventral furrow apical constriction (fig. S4, D and E).

In contrast to wild-type embryos (Fig. 3, B–D), *fog* hemizygous mutants exhibited defects in internalization of mesodermal and posterior midgut cells, which resulted in changes to the morphology of the ventral midline (Fig. 3, E–G) (5). In crosses yielding 25% $mist^{YO17}$ mutant embryos, slightly more than a quarter of the embryos showed clear defects in the internalization of Twist-expressing mesoderm cells or in the morphology of the ventral midline, suggesting that *mist* or one of the other genes deleted in $mist^{YO17}$ is critical for this process (Fig. 3, H–K). We then used *in situ* hybridization for *mist* to genotype individual embryos. As expected, embryonic progeny of $mist^{YO17}$ heterozygous females and wild-type males either had wild-type patterned *mist* expression or low *mist* expression (presumptive $mist^{YO17}$/Y; Fig. 4, A–H and fig. S5). More than 80% of embryos with wild-type *mist* expression showed no gastrulation defects, whereas 95% of embryos with weak *mist* RNA staining exhibited either a failure to fully invaginate mesoderm cells or a defect in the ventral midline, thus correlating *mist* expression with embryonic phenotype (Fig. 4, A–H).

To test the hypothesis that $mist^{YO17}$ gastrulation phenotypes are solely due to the lack of *mist*, we examined whether restoration of *mist* expression could rescue the observed defects. To do so, we took advantage of the fact that although the $mist^{YO17}$ allele deleted the endogenous *mist* promoter, it retained from the P-element a GAL4-regulated upstream activating sequence (UAS) and minimal promoter directed toward the *mist* coding region (fig. S4B). This allowed us to express *mist* under control of specific GAL4 drivers from the endogenous locus. We confirmed that this allele expressed *mist* mRNA and protein by using a driver which is activated in the posterior compartment of each segment in the later embryo (engrailed-GAL4; fig. S3). We then crossed $mist^{YO17}$ heterozygous females containing a maternally expressed GAL4 driver to wild-type males (fig. S5). This cross resulted in loading of GAL4 into eggs during their formation in the ovary, which remained into

embryogenesis. The progeny of this cross had high, ubiquitous accumulation of *mist* RNA throughout most of embryogenesis (Fig. 4, I–J). Strikingly, these embryos showed normal gastrulation (Fig. 4, K and L) in proportions similar to those with wild-type *mist* RNA expression (Fig. 4, C–D and M). This is in contrast to embryos identified as *mist* zygotic mutants by *in situ* hybridization (Fig. 4, E and F), most of which showed gastrulation defects (Fig. 4, G–H and M). These data reinforce the conclusions drawn from our experiments with mixed genotype populations (Fig. 3K). Embryos with ubiquitous *mist* expression still had properly patterned Fog, which presumably allows for the normal organization of their morphogenesis. Embryos that ubiquitously express *fog* but with presumably localized *mist* expression also form a fairly normal ventral furrow (25). These data are consistent with a model in which Mist acts in the Fog pathway during at least some gastrulation events.

To further confirm that loss of *mist* alone can cause gastrulation defects, we injected *mist* dsRNA into preblastoderm embryos and compared them to *fog* dsRNA- and control dsRNA-injected embryos. Control injected embryos rarely exhibited morphogenetic defects, whereas more than 50% of *mist* dsRNA injected embryos displayed disorganization of the ventral midline and/or failure of mesoderm invagination (fig. S6A compared to D–G). These defects resemble those of *fog* dsRNA injected embryos (fig. S6, B–C and G), *fog* mutants, and $mist^{YO17}$ mutants (Fig. 3, E–J). Together, these data suggest that *mist* is the gene responsible for the $mist^{YO17}$ gastrulation defects and that Mist is necessary for *Drosophila* gastrulation.

Of the other genes disrupted in $mist^{YO17}$, only *rok* has a role in morphogenesis. Therefore, it was imperative to test whether gastrulation defects in $mist^{YO17}$ embryos were due to *rok* loss of function. Previous analysis revealed that *rok* is not zygotically embryonic lethal, which suggests that $mist^{YO17}$ defects are not solely caused by loss of Rok (26). Crosses yielding 25% *rok* hemizygous mutant embryos had similar numbers of gastrulation defects to wild-type controls, and fewer than crosses yielding 25% $mist^{YO17}$ hemizygous mutant embryos (Fig. 3K and fig. S7, A–C). Finally, embryonic expression of *rok* under control of a ubiquitous tubulin promoter did not rescue the gastrulation defects of $mist^{YO17}$ mutants (Fig. 3K and fig. S7, D–F), although this construct can rescue *rok* mutant phenotypes (26). These data suggest that *rok* disruption is not the sole cause of the $mist^{YO17}$ embryonic phenotype and further suggests that Mist is essential for proper *Drosophila* gastrulation.

Fog, Mist, and Rho pathway members all contribute to wing and leg morphogenesis

The downstream Fog effector RhoGEF2 also plays an important role in another epithelial folding event, morphogenesis of the wing imaginal disc. Loss of RhoGEF2 in wing discs, which are the precursors of adult wings, leads to aberrant folding patterns (12). Epithelial folds are stochastic in discs with decreased abundance of RhoGEF2, presumably due to spatial constraints of the growing epithelial sheet. There is no evidence for aberrant proliferation or specification in these discs. *RhoGEF2* folding defects are enhanced by either *fog* or *cta* mutation (24). Consistent with roles in wing imaginal disc folding, *fog* mRNA was expressed in this tissue and was enriched in cells forming the folds (Fig. 5A, white arrows). In contrast, past data suggest that adult wing morphogenesis can occur normally in the absence of Fog or Cta (19, 6). We believe there are likely two distinct issues that lead to these contrasting results. First, some defects in disc folding may be corrected later, and are

thus not evident in the adult structure. Second, in the embryo, the Fog-Cta and T48 pathways converge on RhoGEF2 so that the *RhoGEF2* phenotype is stronger than that of any upstream single mutant (10). Thus, it is possible that more than one pathway converges on RhoGEF2 in disc development.

Despite these complications, the imaginal disc epithelium provided an opportunity to explore whether Mist plays a role in adult morphogenesis and further explore places where Fog, Mist, and Rho pathway proteins might regulate epithelial development. We compared *mist* and *fog m*RNA expression patterns in wild-type wing discs. *fog* mRNA was present not only in wing disc folds (Fig. 5A, white arrows), but also in the wing pouch (Fig. 5A, asterisk). *mist* mRNA abundance was also increased in stripes correlating with the folds of the wing disc (Fig. 5B, white arrows). Both mRNAs were specifically enriched on one side of the fold cells, presumably the apical end (Fig. 5, A and B, white arrows), similar to the apical concentration of *fog* RNA in the embryo (11).

We next asked if altering normal expression of Fog pathway components affects wing disc morphogenesis by expressing different constructs using a wing disc-specific driver (A9-GAL4). A fluorescent control construct alone had no effect on imaginal disc morphology (Fig. 5, C and D), but showed the domain of A9 expression (fig. S8). In contrast, Fog overexpression led to disc and adult wing defects (Fig. 5, C and E). To test whether Mist was important for these effects, we manipulated Mist abundance in wing discs using transgenic RNAi. We confirmed strong reduction or increase of *mist* RNA expression compared to controls through *in situ* hybridization in *mist* RNAi or Mist overexpressing imaginal discs (Fig. 5, F and G). *mist* RNAi led to moderate stochastic, abnormal folding patterns in wing imaginal discs (Fig. 5, C and H). Next, we simultaneously expressed ectopic Fog and *mist* RNAi. Reducing Mist abundance substantially rescued the misfolding phenotypes induced by Fog overexpression in both wing discs and adult wings (Fig. 5, C and I). Together these data suggest that Mist and Fog both help regulate wing disc morphogenesis; our data and those of Barrett *et al.* (12) are consistent with the idea that Fog, Mist, and Cta may provide a contributing, although not necessarily essential, input that regulates RhoGEF2 in this tissue.

We further examined the role of Mist in epithelial morphogenesis using the $mist^{YO17}$ mutant. Reducing the abundance of downstream Fog effectors including Rho, RhoGEF2, and Zipper disrupts leg morphogenesis (27, 28). Heterozygosity for $mist^{YO17}$ led to a high frequency of defects in leg morphogenesis (Fig. 5J compared to K–L; M), a phenotype that was enhanced by heterozygosity for *Rho1* (Fig. 5, M–O). Moreover, heterozygosity for *rok* alone did not affect leg morphogenesis (Fig. 5M). These data suggest that Mist, perhaps in concert with Rok, may play a role in leg morphogenesis with other Rho pathway components. Together, our data are consistent with the hypothesis that Mist plays an important role in the Fog pathway during gastrulation as well as a supporting role in imaginal disc morphogenesis.

Discussion

The Fog pathway is a well understood example of how transcriptional programming is translated into cell behavior, but our picture of how this process is regulated was incomplete.

Our data support a model in which the *Drosophila* GPCR Mist can act in the Fog morphogenetic pathway, providing a role for GPCRs in morphogenesis. Mist may function as the sole receptor for Fog. Alternatively, there may be other receptors that act with Fog either as co-receptors with Mist or in different developmental processes. One possibility is the GPCR CG31660, which Matthew *et al*. identified as a candidate by deletion mapping (29). Further detailed analysis of the phenotypes of *fog*, *t48*, *mist*, *cg31660*, and *rhoGEF2* mutants in living embryos, and cell biological and biochemical characterization of the relationship of Mist to other putative proteins in the pathway, will help define the array of cell behaviors controlled by each protein. The embryo also provides a venue to establish the epistatic relationships of Fog and Mist by combining loss-of-function and misexpression of Fog pathway members.

Our data also allow us to complete the connection between the mesoderm transcriptional program driven by the transcription factors Twist and Snail and the cellular machinery involved in triggering epithelial folding (Fig. 6A). Mist is the first downstream transcriptional target of Snail that is required for ventral furrow invagination. Our data, in combination with data from others, provide a model for how the branches of the Twist and Snail regulatory pathway are ultimately integrated, by driving independently patterned, yet overlapping expression of a ligand-receptor pair (Fig. 6B) (5, 11). Twist activates production of Fog and T48 for ventral furrow invagination and reinforces Snail expression in the presumptive mesoderm cells. Snail, in turn, promotes *mist* expression, either directly or indirectly.

We favor a model in which Fog is secreted and activates Mist through autocrine signaling, leading to activation of Cta, recruitment of RhoGEF2 to the apical membrane through T48, and localized contractility through the Rho pathway. It is also possible, however, that Mist acts independently of Fog in different cellular processes, such as basal expansion or cell shortening along the apical-basal axis. Additionally, as noted above, other receptors may mediate some of the effects of Fog. Strikingly, the process can function correctly with either ubiquitously expressed Fog or ubiquitously expressed Mist [our data and (25)]. The co-expression of Fog and Mist may help make the patterned morphogenetic process of ventral furrow formation more robust, with possible subtle effects in timing or coordination. The broader implications of these concepts will be important and exciting to explore in the future.

Materials and Methods

Cell Culture and RNAi

S2 and S2R+ cell lines were obtained from the *Drosophila* Genome Resource Center (Bloomington, IL), and cultivated as described previously (30). S2 cells were maintained in SF900 SFM (Invitrogen, Carlsbad, CA) and S2R+ cells in Sang's and Shield's medium (Invitrogen) supplemented with 5% heat-inactivated FBS (Invitrogen). Double stranded RNAs were produced using Promega (Madison, WI) Ribomax T7 kit according to instructions, or ordered from the *Drosophila* RNAi Screening Center (Boston, MA). Primers used for dsRNA synthesis are as follows and are all preceded by the T7 sequence (5′-TAATACGACTCACTATAGG-3′). Control-fwd: 5′-

TAAATTGTAAGCGTTAATATTTTG-3′ and Control-rev: 5′-AATTCGATATCAAGCTTATCGAT-3′ to amplify a region from the pBluescript plasmid; Cta-fwd: 5′-TGACCAAATTAACTCAAGAACGAAT-3′, Cta-rev: 5′-TTCCAGGAACTTATCAATCTCTTTG-3′; RhoGEF2-fwd: 5′-ATGGATCACCCATCAATCAAAAAACGG-3′, RhoGEF2-rev: 5′-TGTCCCGATCCCTATGACCACTAAGGC-3′; Rho-fwd: 5′-GTAAAACTTGCCTTCTGATTGTCT-3′, Rho-rev: 5′-ATCTGGTCTTCTTCCTCTTTTTGA-3′; Mist1-fwd: 5′-AATTGCAAATTGAGGCCAAG-3′; Mist1-rev: 5′-AGAGCATTGATCGGCTGACT-3′; Mist2-fwd: 5′-CTCCATTGCCGGTGATTG-3′; Mist2-rev: 5′-GGAACGTCCACCAGATGTT-3′. For individual dsRNA treatments, cells at 50–90% confluency in 6- or 12-well plates were treated every other day for 7 days with 10μg/ml of dsRNA. Cells were resuspended and plated on Concanavalin A (MP Biomedicals) coated coverslips, allowed to spread for 1 hour, then treated for 10min with concentrated Fog-conditioned medium or medium harvested from untransfected S2 cells (see below). In Fog-capture experiments all conditions were the same except Fog or control treatments were carried out at 4°C and HL3 and formaldehyde solutions were equilibrated to 4°C but used at room temperature. S2R+ cells were transfected using Effectene Transfection Reagent per the instructions (Qiagen, Dusseldorf, Germany). For dsRNA screening, 96-well plates containing dsRNAs were heated to 95°C for 3min, and then the temperature was lowered 1°C per 30sec to room temperature. 0.2–0.4 μg of a single dsRNA was added to each well of a 96-well plate; then 2.5×10^4 cells were plated in each well and incubated at 25°C for 6 days. Cells were resuspended and 2.5×10^4 cells were plated in each well of a ConA-coated 96-well glass bottom plate (Greiner, Frickenhausen, Germany) for 1 hour prior to Fog treatment. S2 cells were transfected using the Amaxa nucleofector system with Kit V using program G-030 (Lonza, Basel, Switzerland). Statistical significance was determined by first converting probabilities to probits and then performing Student's t-tests. The results were adjusted with the Bonferroni method when multiple comparisons were made using the same data sets. Figures depict probabilities, but P values were determined using probits.

Production of recombinant Fog protein

We engineered a stable Fog-secreting cell line by amplifying the Fog open reading frame and ligating it into the inducible pMT-V5/His A plasmid (Invitrogen). Stable Fog-producing cells were obtained by co-transfecting S2 cells with pMT-Fog-Myc and pCoHygro hygromycin selection plasmid (Invitrogen) followed by antibiotic selection as directed by the manufacturer. Fog producing cells were plated at 70–90% confluency in 150cm^2 flasks for 24 hours, washed two times with Schneider's SFM (Invitrogen), and induced for 48 hours in Schneider's with 100μM $CuSO_4$. Medium was collected and clarified of cells by centrifugation at 4000 × g for 10min. Cleared medium was concentrated 40x in Amicon 30k centrifugal concentration devices (Millipore, Billerica, MA). Concentrated Fog containing medium or similar control medium was diluted 1:1 with fresh Schneider's for use on cells.

Immunofluorescence microscopy of cells

Cells were plated on coverslips treated with ConA, fixed with 4% formaldehyde (EM Sciences, Gibbstown, NJ) in HL3 buffer (70 mM NaCl; 5 mM KCl; 1.5 mM $CaCl_2$-$2H_2O$;

20 mM $MgCl_2$-$6H_2O$; 10 mM $NaHCO_3$; 5 mM trehalose; 115 mM sucrose; 5 mM HEPES; pH to 7.2), and permeablized with PBST or TBST for phosphorylated myosin antibody staining. Cells were blocked with 5% normal goat serum (Sigma-Aldrich, St. Louis, MO) in PBST (or TBST) and stained with antibody diluted into the same solution. Following washing, cells were incubated with secondary antibodies and Alexa488-phalloidin (1:100 dilution; Invitrogen), washed again, and mounted in fluorescence mounting medium (Dakocytomation, Glostrup, Denmark). We acquired images using a CoolSnap HQ CCD camera (Roper Scientific, Ottobrunn, Germany) on a Nikon Eclipse Ti inverted microscope driven by Nikon Elements software (Tokyo, Japan). Photoshop CS4 (Adobe, San Jose, CA) was used to adjust input levels so that the main range of signals spanned the entire output grayscale and to adjust brightness and contrast.

Drosophila tissues

Embryos were collected on apple juice plates supplemented with yeast paste at 25°C, fixed in 4% formaldehyde in PBS/heptane, methanol divitilenized, and stained as above without phalloidin. For Zipper staining embryos were fixed in NaCl/Triton at 100°C. DNA was stained with Hoescht 33342 diluted 1:10,000. In mutant embryo analysis all embryos in a population within a certain range of stages were scored. The percentages of mutant embryos expected and the range of stages examined are indicated in each figure legend.

Wing imaginal discs were collected by picking wandering 3rd instar larvae and dissecting them in PBS, leaving discs attached to the larval cuticles during staining. They were fixed in 4% formaldehyde in PBS with 0.1% Tween-20 and stained as above. Imaginal discs were mounted by dissecting wing discs from the larval cuticles in 70% glycerol in PBS. Abnormal morphology in wing discs was defined by discs having at least two of the following characteristics: bifurcation of a usually single fold, a fold reduced to half or less of its normal length, an extra fold, intersection of two folds, or an obvious bend in a normally straight fold. Abnormal morphology in adult wings was defined by the presence of at least one distinct fold or blister in the wing blade. Statistics for Fig. 3K, 4M, 5C and M, and adult wings were determined by Chi squared test.

Images of embryos and imaginal discs were obtained using a Leica DMI 6000 microscope driven by LAS AF software (Leica Microsystems, Buffalo Grove, IL). Cross-sectioned embryos were prepared as previously described (11) and imaged using a Zeiss LSM 710 and LSM software (Zeiss, Thornwood, NY), or a Vt-Hawk Swept-field confocal and Vox Cell-Scan software (Visitech, Sunderland, UK). Photoshop CS4 (Adobe, San Jose, CA) was used to adjust input levels so that the main range of signals spanned the entire output grayscale and to adjust brightness and contrast.

Immunoblotting

S2 or S2R+ extracts were produced by resuspending cell pellets in PBST. A small amount was reserved to measure protein concentration. After adding SDS-PAGE sample buffer, samples were boiled for 5 minutes. Comparisons were made by normalizing protein loads to immunoblots performed with antibodies to α-tubulin.

in situ hybridization

Probe preparation and *in situ* hybridization for embryos and imaginal discs was performed as described previously (31). *mist* dsRNA probes were made with Digoxygenin-UTP to the entire predicted coding sequence. Fog probes were made with Biotin-RNA labeling kit (Roche) to the sequence amplified with the same T7-Fog primers used to make dsRNA for embryo injection (below). Alkaline phosphatase developing was performed in premixed BCIP/NBT (MP Biomedicals). Fluorescence developing was performed with a Cy5 TSA kit (Perkin-Elmer, Waltham, MA). Alkaline phosphatase-developed tissues were mounted in 70% glycerol in PBS and imaged using a Zeiss Axiophot microscope, Sony 3XDD CCD video camera, and Zeiss Axiovision software. Photoshop CS4 (Adobe, San Jose, CA) was used to adjust input levels so that the main range of signals spanned the entire output grayscale and to adjust brightness and contrast.

Embryo injection

Embryos were prepared as described previously (32), unless noted below. Primers used for dsRNA synthesis are as follows and are all preceded with the T7 sequence. Control-fwd: 5′-TAAATTGTAAGCGTTAATATTTTG-3′ and Control-rev: 5′-AATTCGATATCAAGCTTATCGAT-3′; Fog-Fwd: 5′-ATATTTTTGAGAAGAAATTCCCCAC-3′, Fog-Rev: 5′-CTGTGGTATACTCGTCTTCCTCACT; Mist1 and Mist2: same as used for cell culture. Embryos were injected with a final concentration of 1 μg/μl for all dsRNAs. Embryos were removed from tape using a steady stream of heptane, fixed with 37% para-formaldehyde, and hand-peeled to remove the vitelline membrane. Images were obtained using a Zeiss LSM 710 and LSM software. Photoshop CS4 (Adobe, San Jose, CA) was used to adjust input levels so that the main range of signals spanned the entire output grayscale and to adjust brightness and contrast.

Antibodies

The following antibodies were used in this study: rabbit anti-Myc (Sigma), used at 1:300 dilution; mouse anti-α tubulin monoclonal DM1α (Sigma), used at 1:500; mouse anti-Neurotactin (DSHB), used at 1:50; rabbit anti-Twist (gift from Maria Leptin, European Molecular Biology Laboratory), used at 1:1000; mouse anti-GFP JL8 (Clontech), used at 1:500; sheep anti-Digoxygenin-alkaline phosphatase (Roche, Mannheim, Germany) used at 1:2000; sheep anti-Digoxygenin-POD (Roche) used at 1:50; mouse anti-actin (Millipore) used at 1:1000; rabbit anti-phosphorylated myosin II S19 (Cell Signaling, Danvers, MA) used at 1:100; rabbit anti-Zipper (33) used at 1:500. In addition, streptavidin-alkaline phosphatase (Jackson Immunoresearch, West Grove, PA) was used at 1:1000. Antibodies to Mist were raised in rabbit against a recombinant GST fusion containing the C-terminal 100 residues of Mist by Pocono Rabbit Farm and Laboratories (Canadensis, PA) and used at 1:500 dilution (cells) or 1:5000 (sectioned embryos). Secondary antibodies RhodamineX-conjugated goat anti-rabbit, Cy2-donkey anti-mouse, etc. were all diluted 1:1000 (Jackson Immunoresearch).

P-element excision and determination of mutation

All procedures were carried out at 25°C. Homozygous P-element containing female flies were crossed to males with a marked chromosome expressing transposase. F1 males with mosaic eye and/or body color and the transposase chromosome were chosen and crossed to females with a balancer X chromosome. Single F2 females with the balancer X chromosome, no transposase, and altered eye and/or body color from the F0 females were selected. Each was crossed to males with the same balancer X chromosome to create balanced stocks of excised X chromosomes. These stocks were screened for the lethality of the excisions and for absence of at least one P-element end and non-wild-type *mist* region by PCR. Single dead embryos were chosen from this stock and screened for the absence of amplification of a balancer chromosome-specific product by single embryo PCR. Further PCRs were performed on this hemizygous mutant embryo DNA to determine the extent of the lesion. Once breakpoints were determined, a fragment across the lesion was amplified and sequenced using an Applied Biosystems 3730xl Genetic Analyzer by the UNC – CH Genome Analysis Facility.

For initial screening, genomic DNA was collected from adult flies as suggested by E. Jay Rehm (Berkeley *Drosophila* Genome Project). Single embryos were prepared for PCR by dispensing single fixed embryos into tubes with 10μl Single Embryo Buffer (10mM Tris-HCl, pH 8.2, 1mM EDTA, 25mM NaCl) and incubating at −20°C for 1 hour. After thawing the embryos, Proteinase K was added to a final concentration of 4mM and embryos were incubated at 37°C for 30 min and 95°C for 2 min. Amplifications were performed using Phusion HF Master Mix (Thermo Scientific, Waltham, MA).

Fly stocks

The following fly lines were used in this study: UAS-*mist* dsRNA, UAS-*cta* dsRNA (Vienna *Drosophila* Resource Center), Ubi-*moesin*-GFP (34), *yellow white*, fog^{S4}/FM7 twist-GFP, A9-GAL4, $twist^{1}$/CyO, $snail^{18}$/CyO, rok^{2}/FM7c, tub-*rok*, P{EPgy2}mthl1[EY16157], *Bc*/CyO H{w^{+},Δ2–3}, UAS-CD8-mRFP (II and III), $Rho1^{rev220}$/CyO, matα4-GAL4VP16 (II and III) (from Bloomington Drosophila Stock Center, Bloomington, Indiana), UAS-*fog* (Eric Wieschaus, Princeton University), arm^{XP33} FRT101/FM7 twist-GFP (35). UAS-*mist* flies were made by Gateway cloning (Invitrogen) the coding region of *mist* into the pPW vector (Terence Murphy, Carnegie Institution), which was sent to Best Gene (Chino Hills, CA) for injection and recovery of random transformants. The stock used in these studies has UAS-*mist* inserted on the third chromosome.

Supplementary Material

Refer to Web version on PubMed Central for supplementary material.

Acknowledgments

We thank S. Crews, R. Duronio, B. Goldstein, and K. Slep for feedback on the manuscript. We thank C. Jones for his helpful advice and guidance with statistical analysis. We thank M. Leptin and E. Wieschaus for reagents.

Funding: This work was supported by grants from the NIH (RO1-GM081645 to SLR and RO1-GM47857 to MP) and the Arnold and Mabel Beckman Foundation (Beckman Young Investigator Award to SLR). KAP was supported by funding from the Lineberger Comprehensive Cancer Center.

References and Notes

1. Pilot F, Lecuit T. Compartmentalized morphogenesis in epithelia: from cell to tissue shape. Dev Dyn. 2005; 232:685–694. [PubMed: 15712202]
2. Kasza KE, Zallen JA. Dynamics and regulation of contractile actin-myosin networks in morphogenesis. Curr Opin in Cell Biol. 2011; 23:30–38. [PubMed: 21130639]
3. Leptin M. Drosophila gastrulation: from pattern formation to morphogenesis. Annu Rev Cell Dev Biol. 1995; 11:189–212. [PubMed: 8689556]
4. Sawyer JM, Harrell JR, Shemer G, Sullivan-Brown J, Roh-Johnson M, Goldstein B. Apical constriction: a cell shape change that can drive morphogenesis. Dev Biol. 2010; 341:5–19. [PubMed: 19751720]
5. Costa M, Wilson ET, Wieschaus E. A putative cell signal encoded by the folded gastrulation gene coordinates cell shape changes during Drosophila gastrulation. Cell. 1994; 76:1075–1089. [PubMed: 8137424]
6. Parks S, Wieschaus E. The Drosophila gastrulation gene concertina encodes a G alpha-like protein. Cell. 1991; 64:447–458. [PubMed: 1899050]
7. Izumi Y, Ohta N, Itoh-Furuya A, Fuse N, Matsuzaki F. Differential functions of G protein and Baz-aPKC signaling pathways in Drosophila neuroblast asymmetric division. J Cell Biol. 2004; 164:729–738. [PubMed: 14981094]
8. Wilkie TM, Kinch L. New roles for Galpha and RGS proteins: communication continues despite pulling sisters apart. Curr Biol. 2005; 15:R843–4. [PubMed: 16243026]
9. Rogers SL, Wiedemann U, Häcker U, Turck C, Vale RD. Drosophila RhoGEF2 associates with microtubule plus ends in an EB1-dependent manner. Curr Biol. 2004; 14:1827–1833. [PubMed: 15498490]
10. Kölsch V, Seher T, Fernandez-Ballester GJ, Serrano L, Leptin M. Control of Drosophila gastrulation by apical localization of adherens junctions and RhoGEF2. Science. 2007; 315:384–386. [PubMed: 17234948]
11. Dawes-Hoang RE, Parmar KM, Christiansen AE, Phelps CB, Brand AH, Wieschaus EF. folded gastrulation, cell shape change and the control of myosin localization. Development. 2005; 132:4165–4178. [PubMed: 16123312]
12. Barrett K, Leptin M, Settleman J. The Rho GTPase and a putative RhoGEF mediate a signaling pathway for the cell shape changes in Drosophila gastrulation. Cell. 1997; 91:905–915. [PubMed: 9428514]
13. Häcker U, Perrimon N. DRhoGEF2 encodes a member of the Dbl family of oncogenes and controls cell shape changes during gastrulation in Drosophila. Genes Dev. 1998; 12:274–284. [PubMed: 9436986]
14. Sweeton D, Parks S, Costa M, Wieschaus E. Gastrulation in Drosophila: the formation of the ventral furrow and posterior midgut invaginations. Development. 1991; 112:775–789. [PubMed: 1935689]
15. Brody T, Cravchik A. Drosophila melanogaster G protein-coupled receptors. J Cell Biol. 2000; 150:F83–8. [PubMed: 10908591]
16. Broeck JV. Insect G protein-coupled receptors and signal transduction. Arch Insect Biochem Physiol. 2001; 48:1–12. [PubMed: 11519072]
17. Cronshaw DG, Nie Y, Waite J, Zou YR. An essential role of the cytoplasmic tail of CXCR4 in G-protein signaling and organogenesis. PLoS One. 2010; 11:e15397. [PubMed: 21124917]
18. Leptin M, Grunewald B. Cell shape changes during gastrulation in Drosophila. Development. 1990; 110:73–84. [PubMed: 2081472]
19. Zusman SB, Wieschaus EF. Requirements for zygotic gene activity during gastrulation in Drosophila melanogaster. Dev Biol. 1985; 111:359–371. [PubMed: 3930314]

20. Simpson P. Maternal-Zygotic Gene Interactions during Formation of the Dorsoventral Pattern in Drosophila Embryos. Genetics. 1983; 105:615–632. [PubMed: 17246169]
21. Boulay JL, Dennefeld C, Alberga A. The Drosophila developmental gene snail encodes a protein with nucleic acid binding fingers. Nature. 1987; 330:395–398. [PubMed: 3683556]
22. Seher TC, Narasimha M, Vogelsang E, Leptin M. Analysis and reconstitution of the genetic cascade controlling early mesoderm morphogenesis in the Drosophila embryo. Mech Devel. 2007; 124:167–179. [PubMed: 17267182]
23. Leptin M. twist and snail as positive and negative regulators during Drosophila mesoderm development. Genes Dev. 1991; 5:1568–1576. [PubMed: 1884999]
24. Nikolaidou KK, Barrett K. A Rho GTPase signaling pathway is used reiteratively in epithelial folding and potentially selects the outcome of Rho activation. Curr Biol. 2004; 14:1822–1826. [PubMed: 15498489]
25. Morize P, Christiansen AE, Costa M, Parks S, Wieschaus E. Hyperactivation of the folded gastrulation pathway induces specific cell shape changes. Development. 1998; 125:589–97. [PubMed: 9435280]
26. Winter CG, Wang B, Ballew A, Royou A, Karess R, Axelrod JD, Luo L. Drosophila Rho-associated kinase (Drok) links Frizzled-mediated planar cell polarity signaling to the actin cytoskeleton. Cell. 2001; 105:81–91. [PubMed: 11301004]
27. Halsell SR, Chu BI, Kiehart DP. Genetic analysis demonstrates a direct link between rho signaling and nonmuscle myosin function during Drosophila morphogenesis. Genetics. 2000; 155:1253–65. [PubMed: 10880486]
28. Patch K, Stewart SR, Welch A, Ward RE. A second-site noncomplementation screen for modifiers of Rho1 signaling during imaginal disc morphogenesis in Drosophila. PLoS One. 2009; 4:e7574. [PubMed: 19862331]
29. Mathew SJ, Kerridge S, Leptin M. A small genomic region containing several loci required for gastrulation in Drosophila. PLoS One. 2009; 4:e7437. [PubMed: 19823683]
30. Rogers SL, Rogers GC. Culture of Drosophila S2 cells and their use for RNAi-mediated loss-of-function studies and immunofluorescence microscopy. Nat Protocols. 2008; 3:606–611.
31. Kearney JB, Wheeler SR, Estes P, Parente B, Crews ST. Gene expression profiling of the developing Drosophila CNS midline cells. Dev Biol. 2004; 275:473–492. [PubMed: 15501232]
32. Carthew, RW. A Guide to Gene Silencing. Cold Spring Harbor Laboratory Press; 2003. Cold Spring Harbor Protocols, (2006) modified from RNAi.
33. Kiehart DP, Ketchum A, Young P, Lutz D, Alfenito MR, Chang XJ, Awobuluyi M, Pesacreta TC, Inoué S, Stewart CT, Chen TL. Contractile proteins in Drosophila development. Ann N Y Acad Sci. 1990; 582:233–51. [PubMed: 2192598]
34. Edwards KA, Demsky M, Montague RA, Weymouth N, Kiehart DP. GFP-moesin illuminates actin cytoskeleton dynamics in living tissue and demonstrates cell shape changes during morphogenesis in Drosophila. Dev Biol. 1997; 191:103–117. [PubMed: 9356175]
35. Peifer M, Wieschaus E. The segment polarity gene armadillo encodes a functionally modular protein that is the Drosophila homolog of human plakoglobin. Cell. 1990; 63:1167–78. [PubMed: 2261639]
36. Bellen HJ, Levis RW, Liao G, He Y, Carlson JW, Tsang G, Evans-Holm M, Hiesinger PR, Schulze KL, Rubin GM, Hoskins RA, Spradling AC. The BDGP gene disruption project: single transposon insertions associated with 40% of Drosophila genes. Genetics. 2004; 167:761–81. [PubMed: 15238527]
37. Marygold SJ, Roote J, Reuter G, Lambertsson A, Ashburner M, Millburn GH, Harrison PM, Yu Z, Kenmochi N, Kaufman TC, Leevers SJ, Cook KR. The ribosomal protein genes and Minute loci of Drosophila melanogaster. Genetics. 2007; 8:R216.

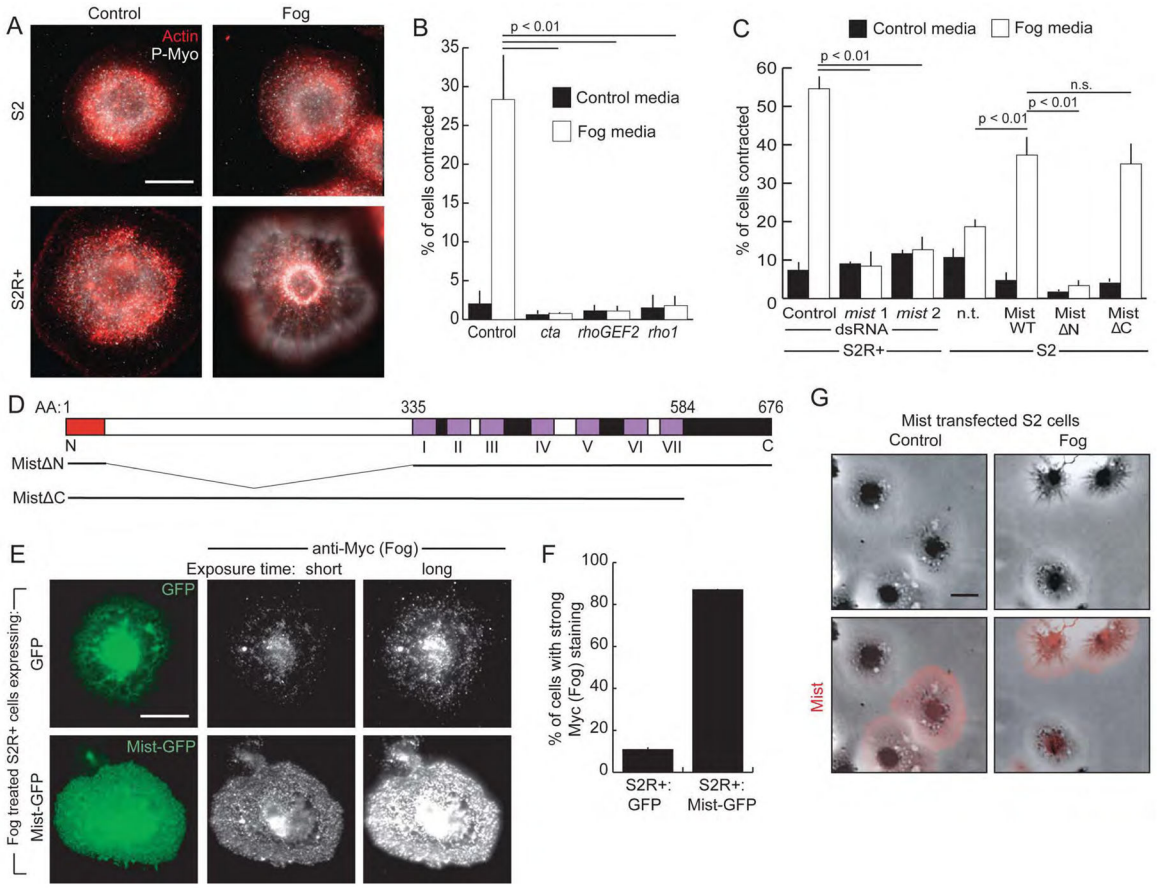

Fig. 1.

Mist transduces Fog signal in cell culture. **A.** S2R+ or S2 cells treated with control- or Fog-conditioned media and stained for actin (red) and phosphorylated myosin (Sqh) (P-Myo; white). **B.** Percentage of S2R+ cells contracted in response to treatment with control- or Fog-conditioned media after RNAi knockdown of Fog pathway components. N=3 sets of cells, with at least 100 cells per condition. **C.** Percentage of cells contracted in response to control or Fog treatment after *mist* knockdown (in S2R+ cells) or overexpression of Mist constructs (in S2 cells). n.t.: not transfected. n.s.: not significant. N=3 sets of cells, with at least 100 cells per condition. **D.** The predicted structure of Mist. Top: 37aa signal sequence (red), 298aa extracellular domain (white), 7 predicted transmembrane domains (purple, numbered with Roman numerals), and a 93aa intracellular domain (black). Extracellular loops are white and intracellular loops black. Bottom: Mist truncations used in C. **E.** S2R+ cells expressing GFP or Mist-GFP were treated with Fog at 4°C and stained for Myc (Fog). Short and long exposures of Myc staining are shown. **F.** Percentage of GFP or Mist-GFP transfected S2R+ cells with Myc (Fog) staining covering the entire cell footprint and clearly reaching to the cell margin (which was defined as strong Myc staining) after treatment with Fog at 4°C. N=3 sets of cells, with at least 100 cells per condition. **G.** S2 cells transfected with untagged Mist, treated with control or Fog media, and stained for Mist (red). Error bars B.,C.,F.=standard deviation. Scale bars in A.,E.,G.: 20μm.

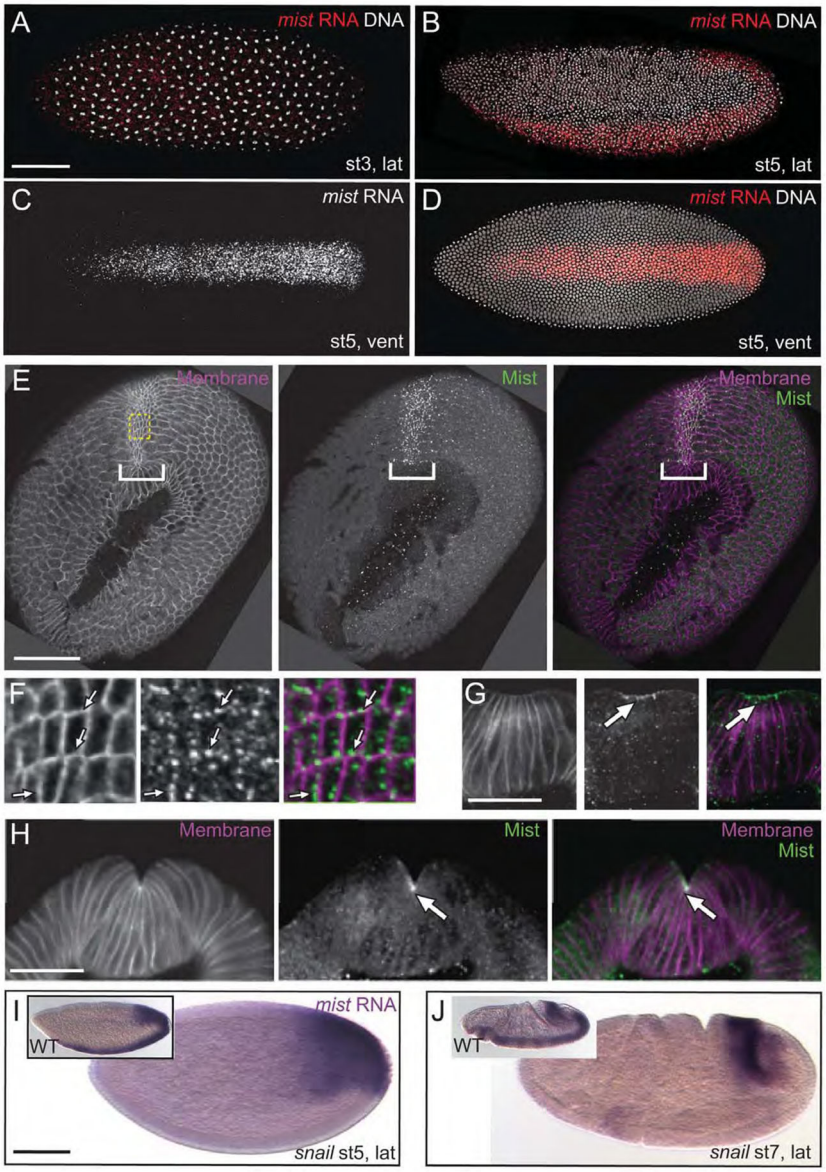

Fig. 2.

mist RNA is found specifically in the ventral furrow downstream of Snail. **A–D.** Fluorescent *in situ* hybridization for *mist* mRNA (red) in wild-type embryos counterstained for DNA (white). Images are representative of 10 embryos per developmental stage. A. Pre-blastoderm stage embryo. B–D. Blastoderm stage embryos before ventral furrow apical constriction. C. *mist* channel alone from D. Anterior is to the left in this and all other embryo figures, and ventral is down in B and toward the viewer in C,D. **E–H.** Mist protein (green) in cross-sectioned embryos undergoing ventral furrow invagination--ventral is to the top and membranes are marked in magenta. Images are representative of 9 embryos. E. Grazing apical cross section. F. Enlarged images of boxed area from E. G. Onset of apical constriction. H. Continuation of apical constriction. Arrows and brackets: Mist is enriched apically in cells of the ventral furrow. **I–J.** *in situ* hybridization to *mist* RNA in *snail* mutant

embryos. Images are representative of 5 embryos per developmental stage. I. Blastoderm stage embryo. J. Gastrulating embryo. Corresponding stages of wild-type embryos are shown in insets. lat: lateral view; vent: ventral view. Scale bar A.,I.: 100μm; E: 50μm; G,H: 25μm.

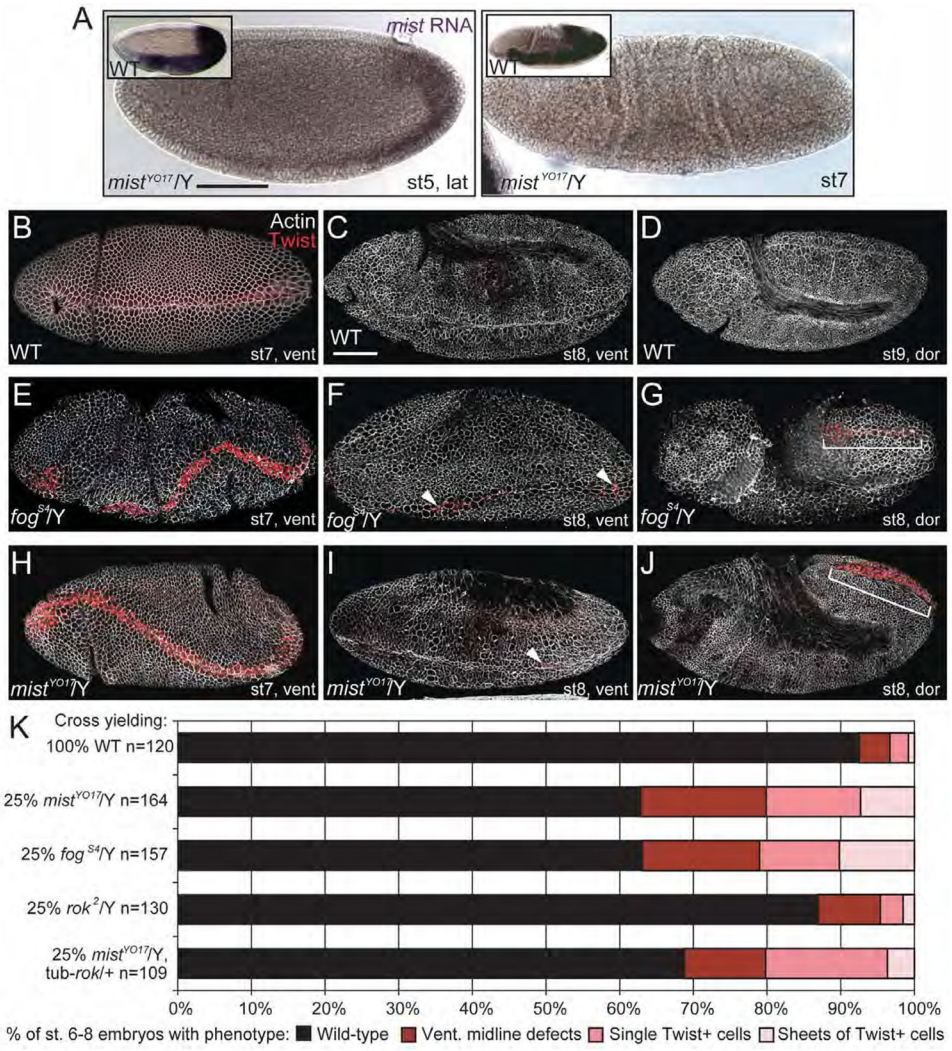

Fig. 3.

Mist is zygotically required for gastrulation. **A.** *in situ* hybridization for *mist* mRNA in $mist^{YO17}$/Y embryos. Corresponding stages of wild-type embryos are shown in insets. Images are representative of at least 7 embryos per developmental stage. **B.–J.** Actin (white) and Twist (red) stained embryos showing the range of gastrulation defects seen. B–D. wild-type embryos. E–G. fog^{S4}/Y embryos. H–J. $mist^{YO17}$/Y embryos. E. and H. Ventral midline defects. F. and I. Single Twist positive cells not internalized (arrowheads). G. and J. Sheets of Twist positive cells not internalized (brackets). **K.** Quantification of gastrulation phenotypes for stage 6–8 embryos as pictured in B–J. rok^{2} gastrulation phenotype distribution is not significantly different from wild-type, and $mist^{YO17}$, fog^{S4}, and $mist^{YO17}$;tub-*rok* distributions differ from wild-type ($p<0.001$). n=number of embryos scored for each condition. vent: ventral view; dor: dorsal view; lat: lateral view. Scale bar A.,C.: 100μm.

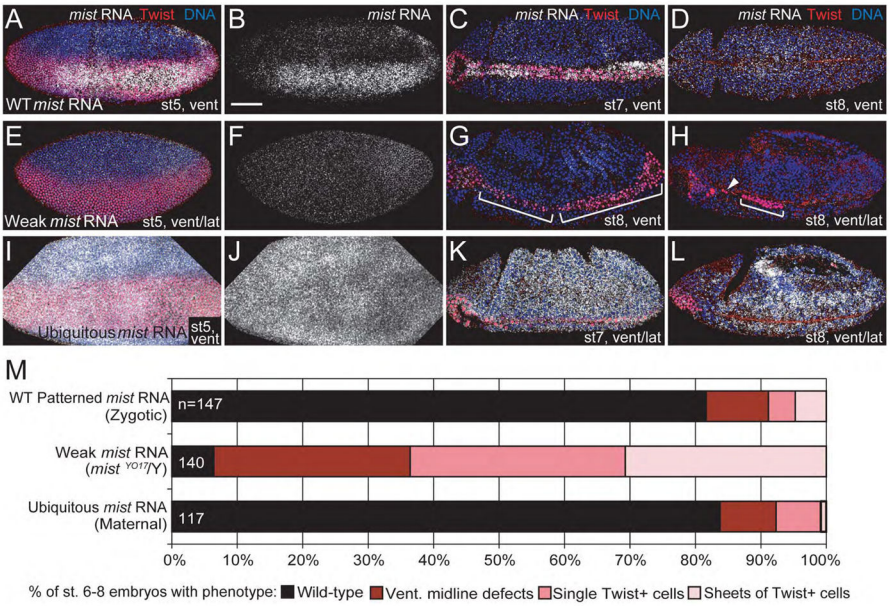

Fig. 4.

mist^{YO17} gastrulation phenotypes require loss of Mist activity. **A–L.** Fluorescent *in situ* hybridization for *mist* RNA (white) seen in embryos from crossing schemes in fig. S5. Twist antibody (red) reveals presumptive mesoderm and DNA is shown in blue. A.–D. Wild-type embryos showing patterned *mist* mRNA expression. E.–H. *mist*^{YO17}/Y embryos show loss of patterned *mist* expression. I.–L. Embryos expressing ectopic *mist* mRNA uniformly (driven maternally). A., E., I. Cellularization stages. B., F., J. *mist* RNA alone from embryos in A.,E.,I., respectively. C.,K. Early germ band extension stages. D.,G.,H., L. Late germ band extension stages. **M.** Quantification of gastrulation phenotypes as done in Fig. 3. Embryos with weak *mist* RNA expression (unrescued *mist*^{YO17}/Y zygotic mutants) have a higher frequency of gastrulation defects compared to *mist*^{YO17} embryos expressing ubiquitous *mist* ($p<0.001$), which are similar in their frequency of defects to control wild-type embryos. arrowhead: single Twist positive cells not internalized. brackets: sheets of Twist positive cells not internalized. n=number of embryos scored for each condition. vent: ventral view; lat: lateral view. Scale bar B.: 100μm.

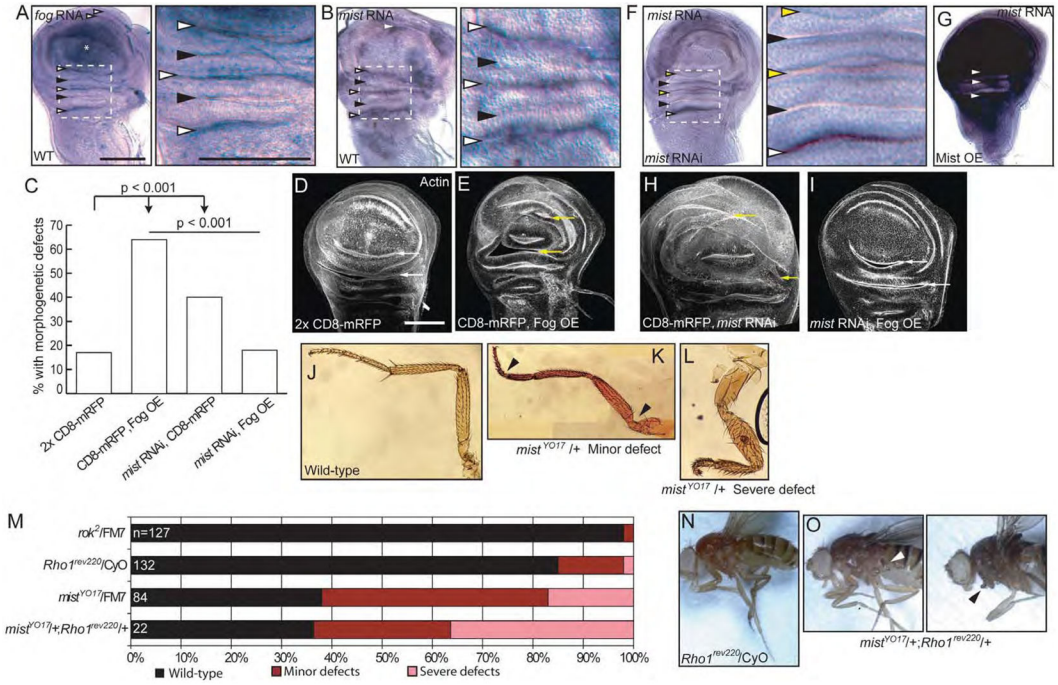

Fig. 5.

Mist and Fog can regulate wing and leg morphogenesis. **A, B.** Left panels: *in situ* hybridization for *fog* (A) or *mist* (B) RNA in wild-type wing imaginal discs. *: RNA in wing pouch. Right panels: Higher magnification of boxed areas in left panels. White arrowheads: *mist* RNA enriched at the apical sides of folds. Black arrowheads: basal sides of fold cells with lower RNA accumulation. Images are representative of at least 10 imaginal discs. **C.** Percentages of wing imaginal discs with morphogenetic defects. Number of imaginal discs scored: 10–15 per condition. **D.,E.** D. Control expression of two copies of CD8-mRFP. E. CD8-mRFP and Fog overexpression. Adult wings of these flies were also malformed: 21/49 adult wings malformed, 43.3%. **F.,G.** *in situ* hybridization for *mist* RNA in *mist* RNAi (F) or Mist overexpressing (G) wing imaginal discs. We chose a relatively morphologically normal wing disc for the *mist* dsRNA panels to allow comparison of *mist* expression in the folds to wild-type. White arrowheads: *mist* RNA enriched at the apical sides of folds. Black arrowheads: basal sides of fold cells with lower RNA accumulation. Yellow arrowheads: fold regions with reduced *mist* RNA. The fold with *mist* RNA in (F), right is outside the expression domain of the driver. Images are representative of 10 imaginal discs per condition. **H.,I.** Actin staining in wing imaginal discs. H. *mist* dsRNA and CD8-mRFP. I. *mist* dsRNA and Fog overexpression. Adult wings from these flies had few morphological defects: 5/108 adult wings malformed, 4.7%. Significantly different from Fog overexpression alone; $p<0.001$. White arrows: proper folds; yellow arrows: misfolding. **J–L.** Examples of a wild-type leg (J) or minor defect (K) and major defect (L) phenotypes in $mist^{YO17}$/+ adults. Arrowheads: leg defects. **M.** Quantification of leg defects in adults of the indicated genotypes according to images in J–L. **N.** Adult $Rho1^{rev220}$/CyO fly with wild-type legs. **O.** Adult $mist^{YO17}$/+;$Rho1^{rev220}$/+ flies. Arrowheads=severely malformed legs. Scale bar A, E: 100μm.

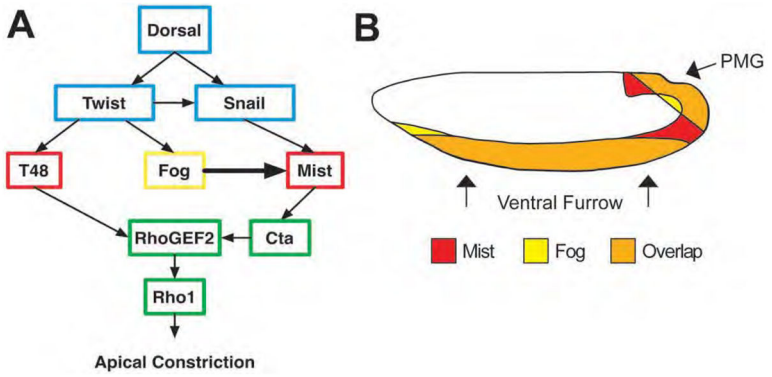

Fig. 6.

Models. **A.** Model for Mist regulation and function within Fog signaling pathway. Colored boxes denote classification of Fog pathway components. Blue: Transcription factor, Yellow: Secreted protein, Red: Transmembrane protein, Green: Cytoplasmic protein. **B.** Schematic of *mist* and *fog* RNA expression in cellularizing embryos. Areas of overlapping expression are where the ventral furrow and posterior midgut invaginate.